PROCEEDINGS OF SCIENCE

Cosmic Ray Electron transport in the external galaxy M51

Julien Dörner,[a,b,*] **Patrick Reichherzer,**[a,b,c] **Julia Becker Tjus**[a,b,d] **and Volker Heesen**[e]

[a] *Theoretical Physics IV, Plasma Astroparticle Physics, Faculty for Physics and Astronomy, Ruhr University Bochum, 44780 Bochum, Germany*

[b] *Ruhr Astroparticle and Plasma Physics Center (RAPP Center), Germany*

[c] *Department of Physics, University of Oxford, Oxford OX1 3PU, UK*

[d] *Department of Space, Earth and Environment, Chalmers University of Technology, 412 96 Gothenburg, Sweden*

[e] *University of Hamburg, Hamburger Sternwarte, Gojenbergsweg 112, 21029 Hamburg, Germany*

E-mail: jdo@tp4.rub.de

Recent measurements of the synchrotron emission of the external galaxy M51 give indirect implications for the cosmic-ray electron (CRE) transport in the interstellar medium. In its face-on geometry, a radial resolved measurement of the star formation rate and the magnetic field strength is possible. Additionally, the diffusion coefficient can be inferred and seems to be energy independent. By modelling the CRE transport considering all relevant energy loss processes, we aim to distinguish the contribution of diffusive and advective transport. Therefore, we use the publicly available transport code `CRPropa3.2` to solve the 3D transport equation. With our best-fit model, the data can be described well. For the best fit, the wind speed followed from the observation of the star formation rate must be decreased by a factor 5. We find that the inner galaxy is dominated by advection and the outer is composed by both spatial diffusion and advection. In general, this approach of modelling face-on galaxies gives insights to the only indirect observable advection profile.

38th International Cosmic Ray Conference (ICRC2023)
26 July - 3 August, 2023
Nagoya, Japan

ICRC2023
38th International Cosmic Ray Conference
The Astroparticle Physics Conference

*Speaker

© Copyright owned by the author(s) under the terms of the Creative Commons Attribution-NonCommercial-NoDerivatives 4.0 International License (CC BY-NC-ND 4.0).

PoS(ICRC2023)231

1. Introduction

In the past decades, the field of multi-wavelength and multi-messenger astronomy evolved significantly, and nearby galaxies that allow for the detection of spatially resolved substructures become more and more important. The observation at different wavelengths reveals information about the population of many of the ingredients needed to describe a spatially resolved cosmic-ray transport model. In particular, information on the 3D magnetic field structures, a differential view on the star formation rate and secondary properties such as the spectral index of cosmic rays, the cosmic-ray diffusion coefficient, as well as the advection velocity of the plasma can be provided for both edge-on [1–3] and face-on [4–7] galaxies. This wealth of data brings 1D transport models beyond their limits as they try to either describe the galaxy in edge-on or face-on geometry as it is observed. This is a useful simplification but it neglects the implications of the 3D structure of the galaxy. The first steps to a realistic 3D model have been done in [7].

In this work, we use the publicly available Monte-Carlo code CRPropa3 [8–10] to solve the 3D transport equation. CRPropa can solve it via the method of stochastic differential equations (SDEs), where the Fokker-Planck equation is converted to a set of SDEs. This is useful here, as the particle densities are derived from the pseudo-particle trajectories. This approach also allows for the inclusion of continuous and catastrophic losses for producing full particle showers in the interaction.

2. Methods

We solve the three-dimensional transport equation [11]

$$\frac{\partial n}{\partial t} = D\nabla^2 n - \vec{v}\cdot\nabla n - \frac{\partial}{\partial E}\left[\frac{\mathrm{d}E}{\mathrm{d}t}n\right] + S \tag{1}$$

for the particle number density n for the case of isotropic diffusion. Here, D is the (scalar) diffusion coefficient, S describes the sources, $\frac{\mathrm{d}E}{\mathrm{d}t}$ is the energy loss term described in Section 2.2, and $\vec{v}$ is the advection velocity of the interstellar medium (ISM) derived from the Star Formation Rate surface Density (SFRD) as described in Section 2.3. In contrast to 1D simulations eq. 1 contains no leakage term, as in the 3D case the leakage of particles to the intergalactic medium (IGM) is described with the boundary conditions. The details of the geometry are discussed in Section 2.4. A detailed description of the numerical methods can be found in [7].

2.1 Diffusion

The interactions of charged CREs with the turbulent magnetic fields in the ISM lead to a diffusive behaviour [11]. This behaviour can be described by the spatial diffusion tensor $\hat{D}$. This tensor can describe anisotropic diffusion, which is believed to significantly determine CRe transport within the magnetic fields present in spiral galaxies [18–21]. An accurate 3D diffusion model would, however, require information about the relationship between parallel and perpendicular diffusion coefficients and knowledge of the three-dimensional magnetic-field structure of M51. Given uncertainties in the latter, we assume isotropic diffusion, keeping in mind that this approach may underestimate in-plane transport and overstate parallel escape.

PoS(ICRC2023)231

In general, the diffusion of CREs in preexisting turbulence can be energy dependent [16, 17], but measurements [12] and previous one-dimensional modelling [6] suggest an energy-independent diffusion coefficient for M51. We note that this may change for different energy ranges for the CREs. In this work we compare the two energy-independent measures, the observational diffusion coefficient $D_{\mathrm{obs}} \approx 2 \cdot 10^{28}\,\mathrm{cm^2\,s^{-1}}$ and the modelling based $D_{\mathrm{mod}} \approx 6 \cdot 10^{28}\,\mathrm{cm^2\,s^{-1}}$. Simulations using two different energy-dependent scenarios can be found in [7]. In the energy-dependent case the prediction from the quasi-linear theory for the energy scaling in a Klomogorov-type turbulence ($D \sim E^{1/3}$) and normalise the value at 4 GeV to the M51 observation or the measured value at Earth ($D_0 \approx 6.1 \cdot 10^{28}\,\mathrm{cm^2\,s^{-1}}$).

2.2 Energy loss

The energy loss of CREs in the ISM is mainly driven by two loss processes, synchrotron radiation and inverse Compton scattering. In our simulation, we apply both losses as a continuous loss following the parametrisation from [6]

$$\frac{\mathrm{d}E}{\mathrm{d}t} = 8 \cdot 10^{17} \left(\frac{E}{1\,\mathrm{GeV}}\right)^2 \left[\frac{U_{\mathrm{rad}}}{1\,\mathrm{eV}} + \frac{6 \cdot 10^{11}}{8\pi} \left(\frac{B}{1\,\mathrm{G}}\right)^2\right] \frac{\mathrm{GeV}}{\mathrm{s}} \quad , \tag{2}$$

where E is the energy, U_{rad} is the energy density of the interstellar radiation field. We assume a constant radiation field with $U_{\mathrm{rad}} = 1\,\mathrm{eV}$. The magnetic field strength $B = B(\vec{r})$ is modelled with a radial component based on measurements [14] and an exponential decrease with the height z above the galactic plane, characterised by the scale height h_b:

$$B(\vec{r}) = B(R) \cdot \exp\left\{-\frac{|z|}{h_b}\right\} \quad . \tag{3}$$

2.3 Advection

The advection velocity is directly coupled to the Star Formation Rate surface Density (SRFD, Σ_{SRF}). The authors of [13] found the relation

$$v_{\mathrm{SFR}}\left(\Sigma_{\mathrm{SFR}}\right) = 10^{3.23}\,\Sigma_{\mathrm{SFR}}^{0.41}\,\frac{\mathrm{km}}{\mathrm{s}} \quad . \tag{4}$$

We use this, together with the measured SFRD [1] (see fig. 1) for the wind profile, assuming a constant speed along the z-axis pointing away from the galactic disc

$$\vec{v} = \mathrm{sgn}(z) \cdot v_{\mathrm{SFR}}\left(\Sigma_{\mathrm{SFR}}(R)\right)\,\vec{e}_z \quad , \tag{5}$$

where $\mathrm{sgn}(x) = x/|x|$ denotes the sign function and v_{SFR} is taken from eq. 4.

2.4 Geometry

To model the geometry of M51 we use a cylinder of radius R_{max} and height h_d. All particles reaching the boundary of the geometry at $R = R_{\mathrm{max}}$ or $|z| = h_d$ are lost the IGM. In this work, we fix the radial extend of the galaxy to $R_{\mathrm{max}} = 15\,\mathrm{kpc}$ and test different models for the scaleheight h_d:

PoS(ICRC2023)231

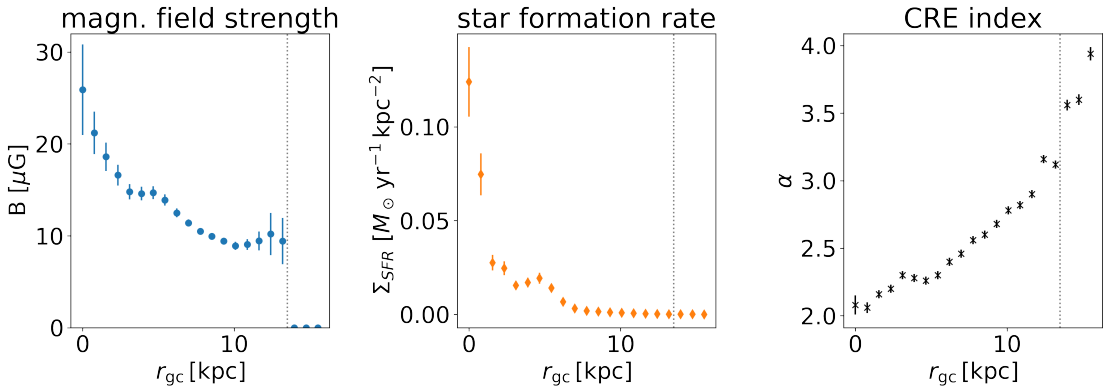

Figure 1: Radial resolved magnetic field strength (left panel), SFRD (middel panel) and CRE index (right panel).

(A) As a first step we test a large-scale height for the galactic height h_d and the magnetic field height h_b with $h_d = h_b = 7\,\mathrm{kpc}$. This case is chosen to demonstrate the impact of the scale-height parameter.

(B) The second geometry model is based on the observed synchrotron emission by [15]. They find an emission height of 1.5 kpc, which corresponds to a disc height of $h_d = 3\,\mathrm{kpc}$ and a magnetic field height of $h_b = 6\,\mathrm{kpc}$.

(C) Mulcahy et al. [6] suggested a radial dependent scale height. This model assumes a constant scale height of 3.2 kpc in the inner galaxy ($R \leq 6\,\mathrm{kpc}$) and 8.8 kpc for the outer galaxy ($R \geq 12\,\mathrm{kpc}$). Those regions are connected by a linear increase of the scale height with the galacto-centric radius R. Here, we use this expression for the disc height and the magnetic field height. Therefore the height can be read as

$$h_d = h_b = h(R) = \begin{cases} 3.2\,\mathrm{kpc} & R \leq 6\,\mathrm{kpc} \\ 3.2\,\mathrm{kpc} + \frac{5.6}{6}(R - 6\,\mathrm{kpc}) & \text{else} \\ 8.8\,\mathrm{kpc} & R \geq 12\,\mathrm{kpc} \end{cases} . \tag{6}$$

3. Results

To compare the simulation with the observed CRE spectral index (see fig. 1, right panel) we bin the observed particle density in galacto-centric rings. Here, we use the same binning as given by the data. Based on that we calculate particle spectra and fit them with a power law in the range $0.5 \leq E/\mathrm{GeV} \leq 6$. In fig. 2 an example for a spectrum is shown. This corresponds to the geometry (C) and the observed energy-independent diffusion coefficient D_{obs}. Also, a correction factor for the wind speed of $f_{\mathrm{adv}} = 0.2$ is used (compare section 3.2). It can be seen that the CRE spectrum follows a power-law in the fitting range, which corresponds to the frequency range of the radio observations. At lower energies, a cut in the index is visible. This is due to a change in the dominant energy loss process. The spectrum in the lower energy part is $\sim E^{-2}$ which corresponds to the

PoS(ICRC2023)231

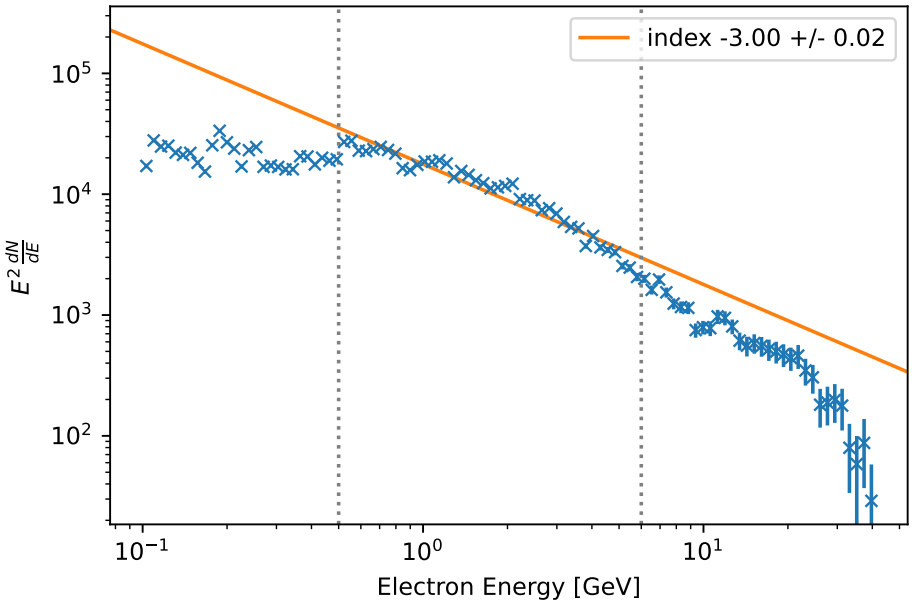

Figure 2: Example of the resulting CRE spectrum with the power-law fit. The grey dotted lines indicate the fitting range for the powerlaw. The data show the radial bin $11.2 \leq R/\,\mathrm{kpc} \leq 12$ assuming a correction factor for the advection speed of $f_{\mathrm{adv}} = 0.2$ (compare Section 3.2).

injection spectrum of the CREs. This implies that the escape of particles is faster than the energy loss.

3.1 Comparing the impact of advection

Figure 3 shows the radial profile of the CRE index α with $dN/dE \sim E^{-\alpha}$ in different geometries. Here, only the simulation for the energy-independent simulations is shown. The simulations have been repeated once including advection (blue marker) and once without advection (green marker). None of these setups fits the data well. All cases, including advection, lead to a spectrum $dN/dE \sim E^{-2}$ close to the injection spectrum. This can be explained by a to strong advection speed, which leads to a much to fast loss of particles.

In the case without advection, the picture changes with the geometry. In the geometry (A), both diffusion cases lead to much to steep spectra. This is somehow expected due to the large extent of the galaxy in this geometry. The large scale height for the escapes leads to a stronger energy loss of the CREs. In the geometry (B) the higher diffusion coefficient D_{mod} fits the inner data, but underestimates the outer part of the galaxy. The lower diffusion coefficient D_{obs} leads to steeper spectra than observed in the inner galaxy. Also, the radial change of the CRE index is not reproduced with this geometry. The radial changing geometry (C) leads to the best agreement of all setups neglecting advection. The observed diffusion coefficient D_{obs} can reproduce the shape of the radial profile, although the CRE index is too high in general. The higher diffusion coefficient D_{mod} matches the shape of the inner profile quite well. In the outer part of the galaxy ($r \gtrsim 6\,\mathrm{kpc}$) the increase of the spectral index is a little bit too small. Compared to the simulation in [6], which

PoS(ICRC2023)231

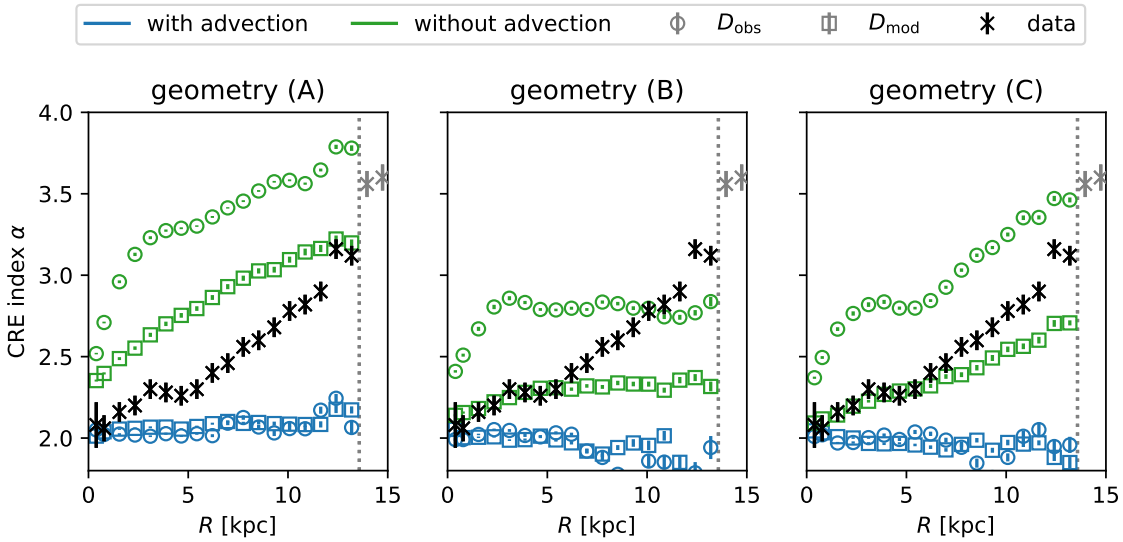

Figure 3: Cosmic Ray Electron index as a function of the galacto centric radius R. The panels represent the different geometries (see Section 2.4).

uses a similar setup for a 1D case, this simulation show a larger difference to the data. The reason for this disagreement of the models can be the change from one-dimensional to three-dimensional modelling and the difference in the observational data used for the simulation/analysis. In our work, we use the most recent data from [14] for the magnetic field.

3.2 Reducing the wind velocity

As shown before the wind velocity based on the SFRD leads to a much too fast escape of CRE. Therefore, a new normalisation of the relation in eq. 4 is introduced by multiplying a factor f_{adv}. We test values in the range $0.1 \leq f_{\mathrm{adv}} \leq 1$ in steps of 0.1 and $f_{\mathrm{adv}} \in \{10^{-4}, 10^{-3}, 10^{-2}\}$. After the simulation, the reduced χ^2 difference between the simulation and the observed CRE index is calculated as

$$\chi^2_{\mathrm{red}} = \frac{1}{n-1} \sum_{i=1}^{n} \frac{\left(\alpha_i^{\mathrm{obs}} - \alpha_i^{\mathrm{sim}}\right)^2}{\sigma_i^2}, \tag{7}$$

where α_i is the observed or simulated CRE index in the i-th bin and σ_i the corresponding observational error. The resulting values are shown in figure 4. The values show a clear preference of the geometry (C) with the lower diffusion coefficient D_{obs}. For this case, the radial profile of the CRE index is shown in figure 5. The preferred reduction is $f_{\mathrm{adv}} = 0.2$, with a relatively sharp minimum. This does not allow for a large variation of the reduction factor.

4. Conclusion

We show that three-dimensional transport modelling of face-on galaxies opens the possibility of investigating the galactic winds. We apply this approach to model the external galaxy M51. Our best-fit model has the following setup:

PoS(ICRC2023)231

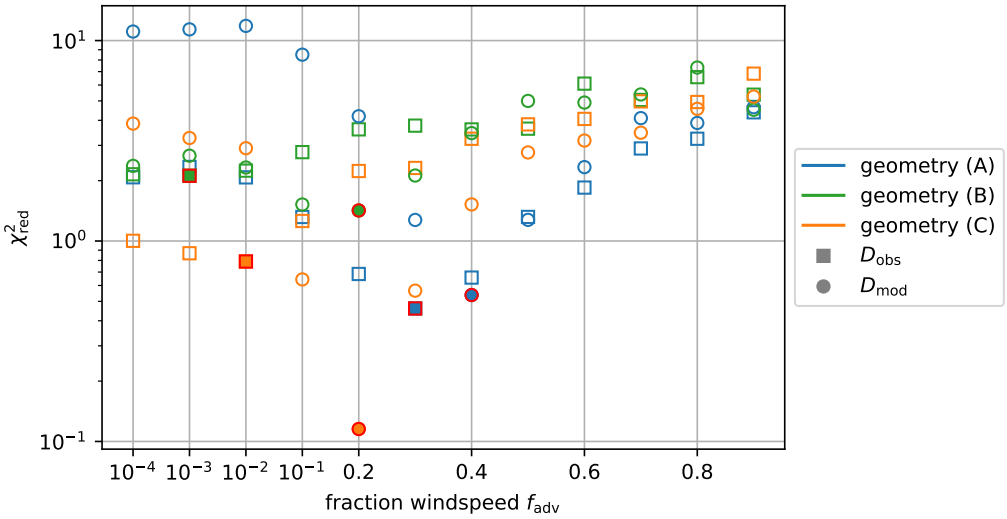

Figure 4: Reduced χ^2 values for different reduction factors f_{adv} of the advection speed. The minima of each geometry and diffusion coefficient combination are marked by a filled marker with a red edge.

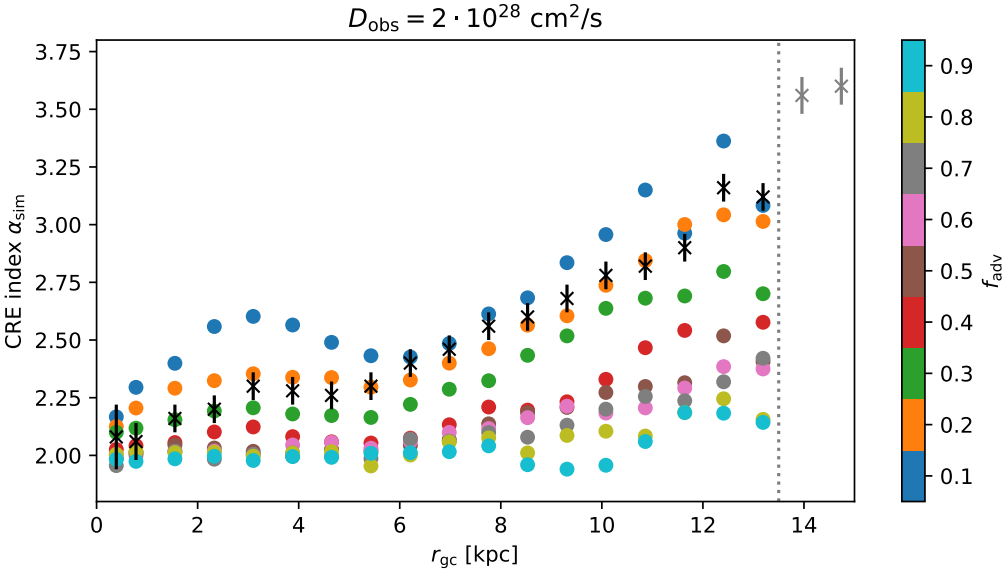

Figure 5: Radial profile of the CRE index. Here the geometry (C) and the observation-based diffusion coefficient D_{obs} is used. The colour denotes different values of the reduction factor f_{adv}.

1. The diffusion coefficient is energy independent with $D = 2 \cdot 10^{28} \mathrm{cm}^2\,\mathrm{s}^{-1}$. This value is based on recent measurements by [12].

2. The geometry of M51 is modelled in a cylindrical geometry with radial extend of $R_{\mathrm{max}} = 15\,\mathrm{kpc}$ and a radial dependent scale height. We use a constant scale height $h = 3.2\,\mathrm{kpc}$ for the inner galaxy ($R \leq 6\,\mathrm{kpc}$) and $h = 8.8\,\mathrm{kpc}$ for the outer galaxy ($\geq 12\,\mathrm{kpc}$). In between the scale height increases linearly.

PoS(ICRC2023)231

3. The advection speed followed by the SFRD has to be reduced by a factor of 5.

Depending on the escape timescale due to diffusion and advection a break in the spectrum of the CREs is expected (see e.g. fig. 2). Future observations over a larger energy range may hint at this break and further constrain the geometry of M51.

References

[1] V. Heesen, M. Krause, R. Beck *et al.*, MNRAS, 476, 158 (2018)

[2] A. Miskolczi, V. Heesen, C. Horellou *et al.*, A&A, 622, A9 (2019)

[3] G.H. Heald, V. Heesen, S.S. Sridhar *et al.*, MNRAS, 509, 658-684 (2021)

[4] E.J. Murphy, G. Helou, J.D.P. Kenney *et al.*, ApJ, 678, 828 (2008)

[5] F.S. Tabatabei, E. Schinnerer, E.J. Murphy *et al.*, A&A, 552, A19 (2013)

[6] D. Mulcahy, A. Fletcher, R. Beck *et al.*, A&A, 592, A123, (2016)

[7] J. Dörner, P. Reichherzer, J. Becker Tjus *et al.*, A&A 669, A111 (2023)

[8] R. Alves Batista, A. Dundovic, M. Erdmann *et al.*, JCAP, 05, 038 (2016)

[9] L. Merten, J. Becker Tjus, H. Fichtner *et al.*, JCAP, 06, 046 (2017)

[10] R. Alves Batista, J. Becker Tjus, J. Dörner *et al.*, JCAP, 09, 035 (2022)

[11] J. Becker Tjus, L. Merten, Physics Reports, 872, 1-98 (2020)

[12] V. Heesen, E. I. Buie, C. J. Huff *et al.*, A&A, 622, A8 (2019)

[13] V. Heesen, Ap&SS, 366, 117 (2021)

[14] V. Heesen, T. L. Klocke, M. Brüggen *et al.*, A&A, 669, A8 (2023)

[15] M. Krause, J. Irwin, T. Wiegert *et al.*, A&A, 611, A72, (2018)

[16] J. Giacalone, R.R. Jokipii, ApJ, 520, 204 (1999)

[17] P. Reichherzer, J. Becker Tjus, E. G. Zweibel *et al.*, MNRAS, 498, 5051 (2020)

[18] F. Effenberger, H. Fichtner, K. Scherer *et al.*, A&A, 547, A120 (2012)

[19] S.S. Cerri, D. Gaggero, A.Vittino *et al.*, JCAP, 10, 019 (2017)

[20] P. Reichherzer, L. Merten, J. Dörner *et al.*, SN Appl. Sci. 4, 15 (2022)

[21] P. Reichherzer, J. Becker Tjus, E. G. Zweibel *et al.*, MNRAS, 514, 2658 (2022)

PoS(ICRC2023)231